International Journal of Microwave and Wireless Technologies

cambridge.org/mrf

Design and implementation of a circularly polarized rectenna for efficient RF energy harvesting

Ranjana Kumari[1], Ankit Sharma[1], Ruchi Agarwal[2] and Sachin Kumar[1]

[1]Department of Electronics and Communication Engineering, Galgotias College of Engineering and Technology, Greater Noida, India and [2]Department of Electronics and Communication Engineering, Pranveer Singh Institute of Technology, Kanpur, India

Research Paper

Cite this article: Kumari R, Sharma A, Agarwal R, Kumar S (2026) Design and implementation of a circularly polarized rectenna for efficient RF energy harvesting. *International Journal of Microwave and Wireless Technologies* **18**(4), 593–604. https://doi.org/10.1017/S1759078726103158

Received: 22 June 2025
Revised: 31 March 2026
Accepted: 3 April 2026
First published online: 21 July 2026

Keywords:
antenna; energy harvesting; ISM band; rectenna; rectifier

Corresponding author: Sachin Kumar; Email: gupta.sachin0708@gmail.com

Abstract

This paper presents a rectenna with a pentagonal-shaped circularly polarized (CP) antenna and a rectifier for radio frequency (RF) energy harvesting in the industrial, scientific and medical (ISM) (2.4 GHz) band. The antenna gain is increased by incorporating a frequency selective surface (FSS) over the patch of the antenna. A rectifier with a series topology and a T-matching network is used to translate RF energy received via the CP antenna to direct current power. The rectifier employs a Schottky diode (HSMS-2860) for rectification, achieving a peak conversion efficiency of 56.5% and delivering an output voltage of 238 mV at an input power of −10 dBm across a 1 kΩ load. Also, a unique 3D pentagonal array structure is presented, which consists of five FSS-based antenna elements, each with a 72° coverage angle. The 3D pentagonal antenna array allows for 360° collection of ambient signals, with the CP antenna sensing RF signals in the full azimuth plane, making it suitable for efficient RF energy harvesting.

Introduction

Energy scavenging, also acknowledged as energy harvesting, is the process of collecting, converting, and making use of ambient energy [1]. A typical configuration of a radio frequency (RF) energy harvesting comprises an antenna and a rectifier [2, 3]. The rectenna is comprised of the impedance matching network, rectifier, power management unit, and load. The antenna senses RF signals and sends them to the rectifier via a matching network, which transforms them into a direct current (DC) output [4, 5]. The rectifier consists of diodes that convert sinusoidal signals into DC [6, 7]. The DC power can be used to directly power low-power devices or charge batteries. The matching network ensures maximum power transmission by minimizing signal reflections and matching the impedance of the antenna and rectifier [8, 9].

Recently, several rectenna arrangements have been reported for ambient RF energy harvesting. In paper [10], patch antennas were used for energy harvesting; however, the extremely low RF power density of the surrounding limits the amount of power that can be harvested, resulting in lower gain. In paper [11], a rectenna with a rhombus-shaped antenna and a rectifier with a two-line pi-impedance matching network, including DC combining, were proposed to improve conversion efficiency. In paper [12], a metal wall-loaded wideband cross-dipole antenna was reported with an impedance matching network to support the rectifier in achieving high conversion efficiency. Antenna arrays with circular polarization provide better signal reception quality in different orientations, improving RF signal sensing in challenging situations, and allowing greater penetration through barriers [13, 14]. In paper [15], two rectifier topologies covering the sub-6 GHz range were proposed. Design-1 contains a rectifier and a dual transmission line-based matching network to increase rectifier performance. Design-2 included a rectifier circuit with a matching network formed using a multi-stepped transmission line for wide frequency coverage. In paper [16], the rectifier was connected to a dual-band impedance matching network, and the receiving antenna was a wideband monopole. The antenna demonstrated a wide operational bandwidth by using a tapered feed and engraving a cross-shaped groove on the ground surface. In paper [17], a broadband rectifier and a microstrip antenna array were proposed, wherein two sets of arc-shaped slots were loaded near the edge of the circular patch to obtain dual-band response. However, the above-mentioned rectenna designs have a number of shortcomings including low efficiency, bigger size, complex geometry, and environmental variability. To overcome these challenges, a multidisciplinary approach is required, which includes straightforward antenna and rectifier designs, better impedance matching between them, and power management strategies.

© The Author(s), 2026. Published by Cambridge University Press in association with The European Microwave Association.

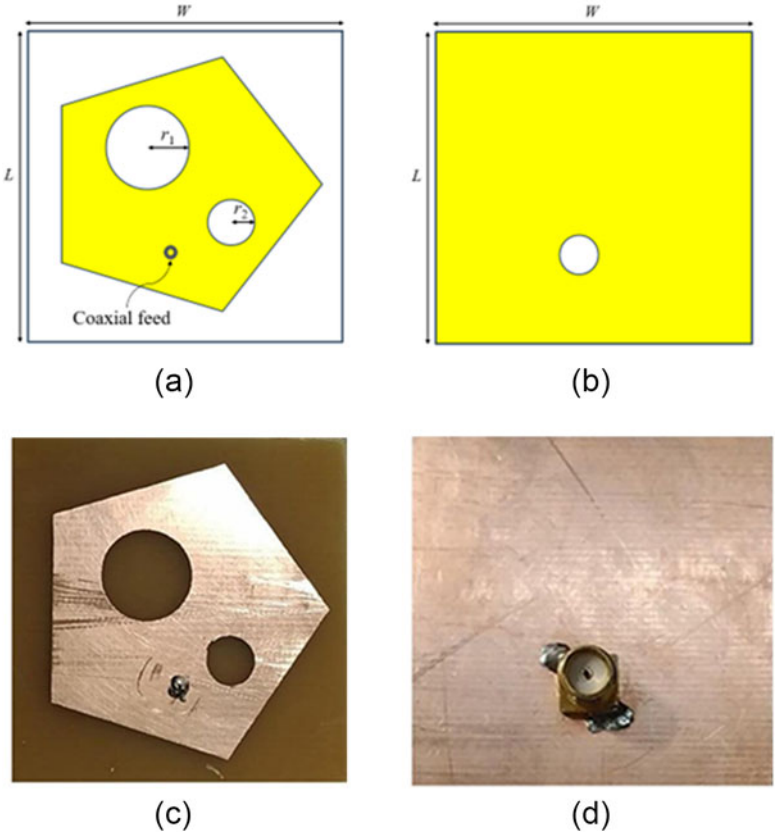


Figure 1. Proposed pentagonal-shaped patch antenna: (a) forward-facing view, (b) backward view, (c) photograph of the forward-facing view of the prototype antenna, and (d) photograph of the backward view of the prototype antenna ($L = W = 40$ mm, $r_1 = 5.2$ mm, $r_2 = 2.8$ mm).

High power conversion efficiency (PCE) is very important in rectennas, which can be achieved by matching the load to the rectifier and blocking the higher-order harmonics produced by the diode using a low-pass filter [18]. In papers [19, 20], circularly polarized (CP) antennas with frequency selective surface (FSS) layers were proposed to achieve high gain. FSS structures can focus incoming RF energy toward the rectenna, effectively improving the directivity and gain of the sensing antenna. However, the above-mentioned FSS-based rectenna designs showed limited bandwidth, linear polarization, and complex architecture. Therefore, a rectenna with a simple design, circular polarization, and a robust impedance matching network is required to enhance the RF-to-DC conversion efficiency.

This paper presents a rectenna that consists of a CP pentagonal-shaped antenna covered with FSS and a rectifier for efficient energy harvesting. The pentagonal patch of the antenna is loaded with two slots to achieve circular polarization. The pentagonal geometry is chosen due to its inherent benefits, including reduced size and potential for improved impedance matching capabilities. The rectifier uses HSMS-2860 diodes and a series topology, which allows for a compact design. A T-matching network is employed to convert the maximum quantity of power from the source to the load. The maximum efficiency of 56.5% at 2.4 GHz with −10 dBm input power is recorded. Furthermore, a 3D antenna array configuration is proposed, along with FSS. The array consists of five antenna elements, each with a 72° coverage angle. The 3D pentagonal antenna array allows for 360° collection of ambient signals, making it suitable for real-world implementation.

Antenna configuration

Patch antenna design

Figures 1(a) and (b) show the suggested antenna, which consists of a pentagonal-shaped patch fed through a coaxial feed. The pentagon shape is chosen as it offers a more compact design than conventional shapes such as rectangular, circular, or elliptical. Also, the pentagon geometry offers flexibility to incorporate extra elements such as slots, notches, or loading mechanisms, allowing for performance optimization. The side length of the pentagonal-shaped patch antenna is calculated as

$$s = a_{eff}\sqrt{5 - 2\sqrt{5}} \tag{1}$$

$$a_{\text{eff}} = \frac{1.8412c}{2\pi f_{\text{r}}\sqrt{\varepsilon_{\text{eff}}}}, \tag{2}$$

$$\varepsilon_{eff} = \frac{\varepsilon_r + 1}{2} + \frac{\varepsilon_r - 1}{2}\left(1 + 12\frac{h}{D_p}\right)^{-1/2} \tag{3}$$

where c is the velocity of light in vacuum, f_{r} is the resonance frequency, ε_{r} is the relative permittivity, h is the thickness of the substrate, and D_{p} is the diameter of the pentagon.

The pentagonal-shaped radiating antenna is incorporated with two slots to enhance bandwidth and enable circular polarization. The antenna is modelled using CST Microwave Studio software and fabricated on the FR-4 substrate with a dielectric constant (ε_{r}) of 4.4, loss tangent (tan δ) of 0.02, and a thickness (h) of 1.6 mm. Figures 1(c) and (d) show the prototype of the designed pentagonal-shaped antenna.

https://doi.org/10.1017/S1759078726103158 Published online by Cambridge University Press

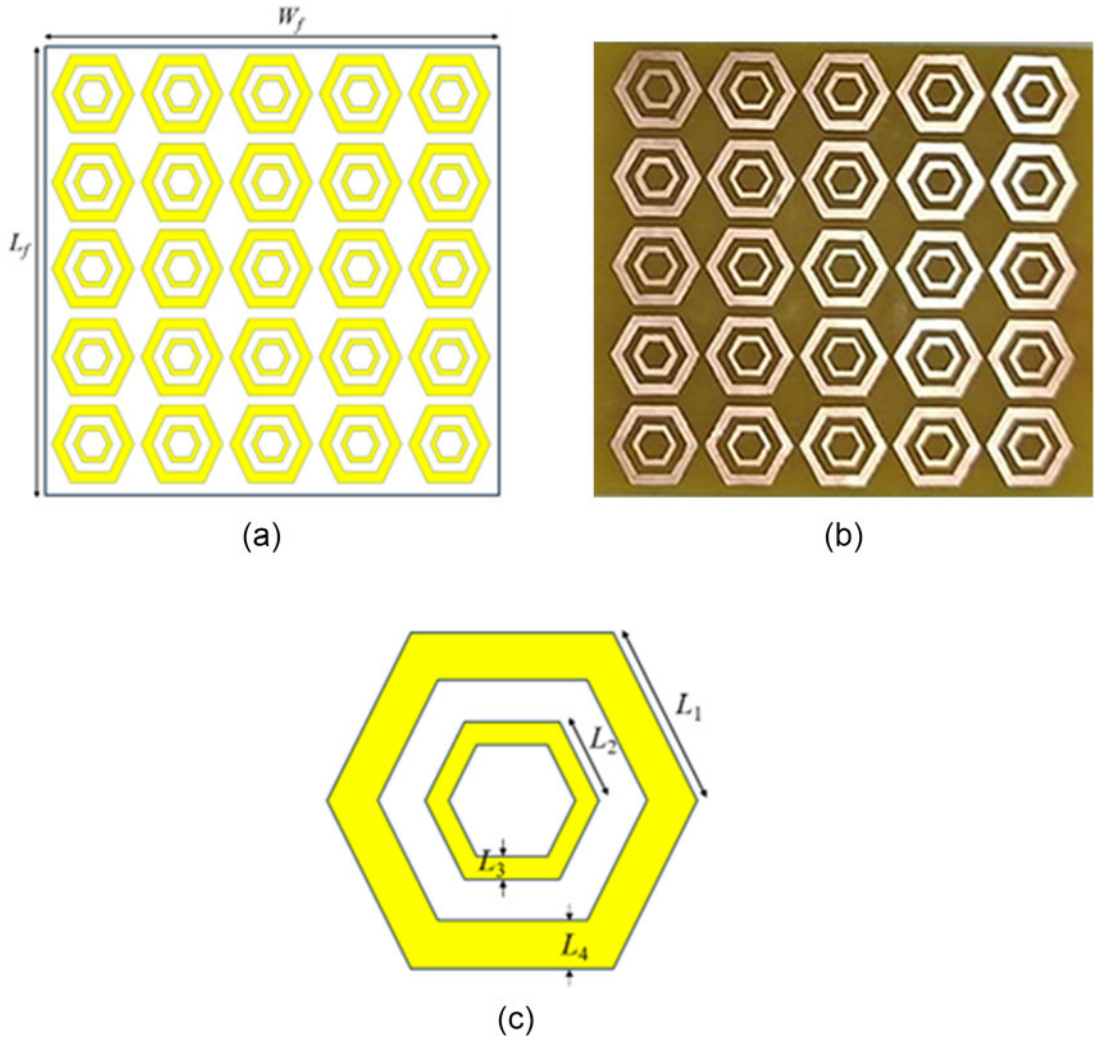


Figure 2. Proposed FSS layer: (a) schematic, (b) photograph of the FSS layer prototype, and (c) unit cell ($L_1 = 4$ mm, $L_2 = 2$ mm, $L_3 = 1$ mm, $L_4 = 0.5$ mm).

FSS layer

Figure 2(a) shows the schematic of the designed FSS array. In the proposed pentagonal-shaped patch CP antenna, FSS plays an important role in increasing the antenna gain. The FSS unit cell is made up of two concentric hexagonal-shaped rings, as illustrated in Figure 2(c). Traditional rectenna configurations are often inefficient in capturing RF signals due to their inherent polarization sensitivity, as noted in previous studies [21]. The length (λ_r) of FSS elements can be calculated as

$$\lambda_r = 2p - 2g + w. \tag{4}$$

The distance between the centers of adjacent hexagonal unit cells is referred to as pitch (p). The outer hexagon size (L_1) has been used to derive the pitch, which is $p = 2 \times L_1$. The gap (g) denotes the space between two adjacent unit cells, and (w) is the trace width of the metallic conductive strip used to make hexagonal ring.

The FSS elements, which have been carefully engineered for maximum performance, allow for selective alteration of the frequency response and polarization of incoming electromagnetic waves. The FSS layer is printed on the FR-4 substrate with dimensions ($W_f = 50$ mm $\times$ $L_f = 40.4$ mm) and a height of 1.6 mm, designed to function efficiently at ISM (2.4 GHz) band. The precise engineering ensures that the FSS layer within the rectenna system functions optimally, enhancing its ability to capture ambient signals. Figure 2(b) shows the prototype of the designed FSS layer.

Integration of patch antenna and FSS

Figure 3(a) depicts the proposed pentagonal-shaped patch antenna integrated with the FSS layer. The optimal gap between the FSS layer and the proposed CP antenna is calculated using rigorous simulations. Maintaining a space between the FSS and the suggested antenna is critical to ensuring the seamless integration and functionality of the FSS-based antenna, allowing for the achievement of desired operational results. Figures 3(b) and (c) display the side and back views of the fabricated antenna with the FSS layer. Figure 3(d) depicts measurement of the antenna in an anechoic chamber with and without FSS.

Figures 4(a), (b), and (c) present the measured and simulated reflection coefficients, axial ratio, and gain of the antenna with and without FSS layer, respectively. The operational frequency does not significantly shift with the FSS layer, indicating no changes in the resonant properties of the antenna. This observation confirms

https://doi.org/10.1017/S1759078726103158 Published online by Cambridge University Press

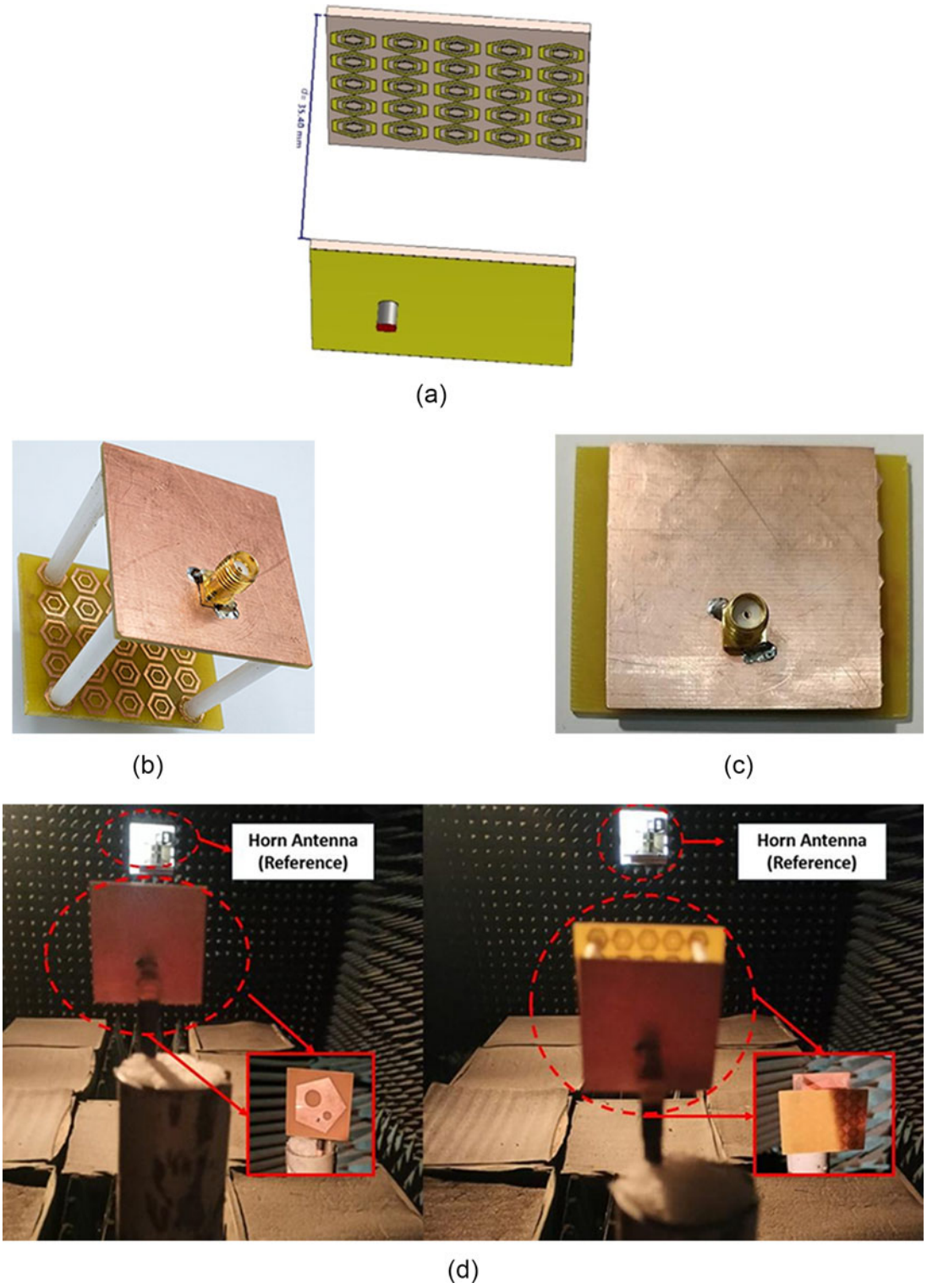


Figure 3. (a) Schematic of reported antenna with FSS plane, (b) side view of prototype with FSS plane, (c) back view of designed prototype with FSS layer, and (d) measurement of reported prototype in an anechoic chamber with and without FSS.

the ability of the FSS structure to interact with incident waves at various angles of arrival [22, 23]. The predicted bandwidth of the antenna is 140 MHz, demonstrating wide performance.

Additionally, it is clear that the addition of the FSS layer has no discernible effect on the axial ratio (dB) of the suggested antenna. At 2.4 GHz, the axial ratio is consistently less than 3 dB, as shown in Figure 4(b), confirming the circular polarization characteristics. Also, the FSS layer increases antenna gain significantly, from 1.12 dBi to 2.22 dBi, as demonstrated in Figure 4(c). Moreover, due to dielectric and conductor losses in the FR-4 substrate, the

https://doi.org/10.1017/S1759078726103158 Published online by Cambridge University Press

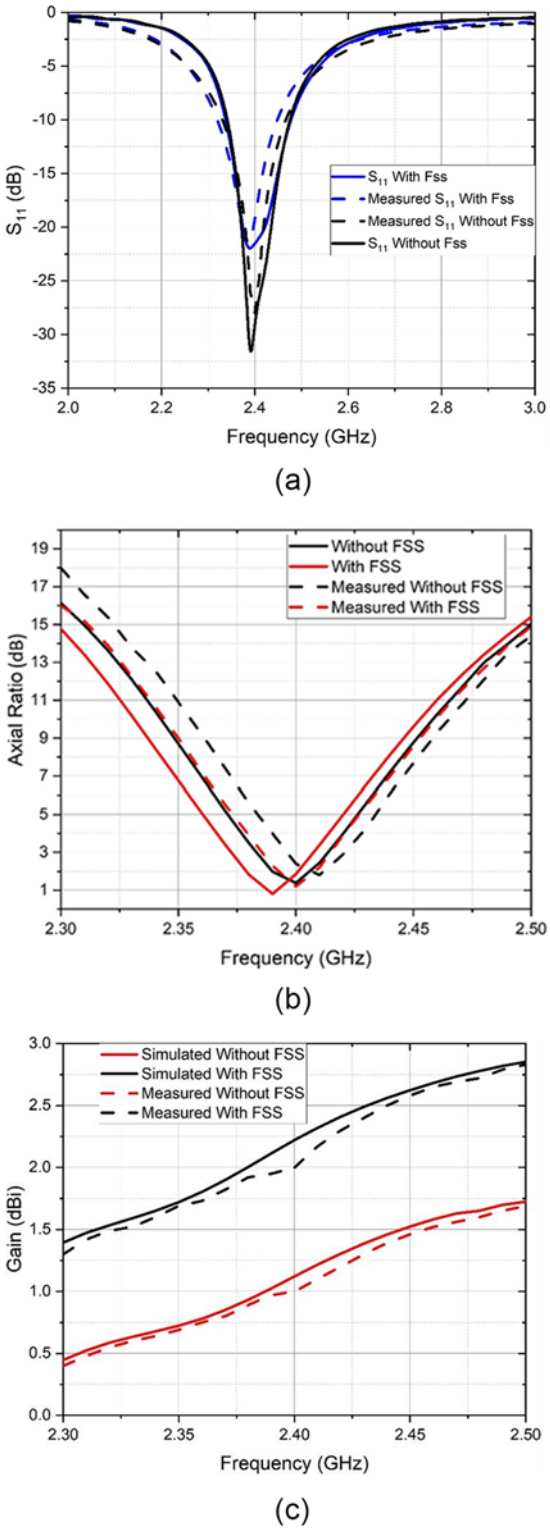


Figure 4. Results of the antenna with and without FSS layer: (a) reflection coefficients, (b) axial ratio, and (c) gain.

antenna without the FSS achieves a maximum radiation efficiency of 65%, whereas with the FSS layer, the efficiency increases to 74% at 2.4 GHz because the FSS suppresses surface-wave modes and enhances broadside radiation. Thus, the FSS compensates for

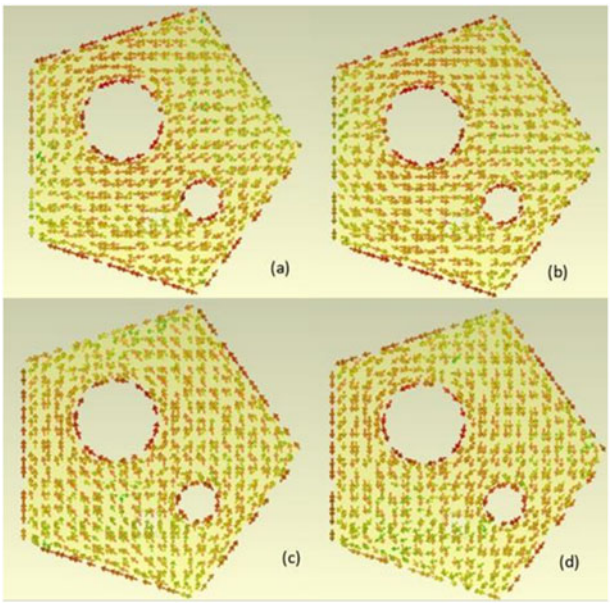


Figure 5. Surface current of the antenna at 2.4 GHz: (a) $\varphi = 0°$, (b) $\varphi = 90°$, (c) $\varphi = 180°$, and (d) $\varphi = 270°$.

the FR-4 losses, improving overall radiating performance at the operating frequency. FR-4 was chosen for this work because it is inexpensive and widely available, making the design suitable for low-cost applications.

Figure 5 depicts the surface current of the pentagonal-shaped radiating element at 2.4 GHz at angles $\varphi = 0°$, $\varphi = 90°$, $\varphi = 180°$, and $\varphi = 270°$. As the electric field vector rotates in a clockwise direction, the antenna demonstrates a right-hand circular polarization (RHCP) pattern, as illustrated in Figures 5(a–d). The suggested antenna design provides robust circular polarization performance at ISM 2.45 GHz band, validating its reliability as a sensing antenna for RF energy harvesting [24]. This eliminates the need to align the proposed antenna with the RF sources, which is important for collecting energy from different sources of variable polarization.

The radiation patterns are measured with a reference standard horn antenna in an anechoic chamber, as displayed in Figure 3(d). The controlled environment provides immunity from external electromagnetic interference while also reducing the emission of electromagnetic waves into the environment. Figures 6(a) and (b) display the measured and simulated RHCP and left-hand circular polarization (LHCP) radiation shape of suggested pentagonal-shaped antenna at 2.4 GHz frequency, $\varphi = 0°$ and $\varphi = 90°$, respectively. The 2D pattern results show that the obtained values of the LHCP curves are less than the values of the RHCP curves, indicating that the proposed antenna is RHCP.

Proposed rectifier

This section describes the design and implementation of the rectifier at 2.45 GHz. Figure 7 illustrates the schematic of the proposed rectifier, which is simulated using Keysight ADS software. The rectifier model makes use of the HSMS-2860 diode due to its low-power operation and series topology, which ensures cost-effective fabrication and compact design. The proposed rectifier is

https://doi.org/10.1017/S1759078726103158 Published online by Cambridge University Press

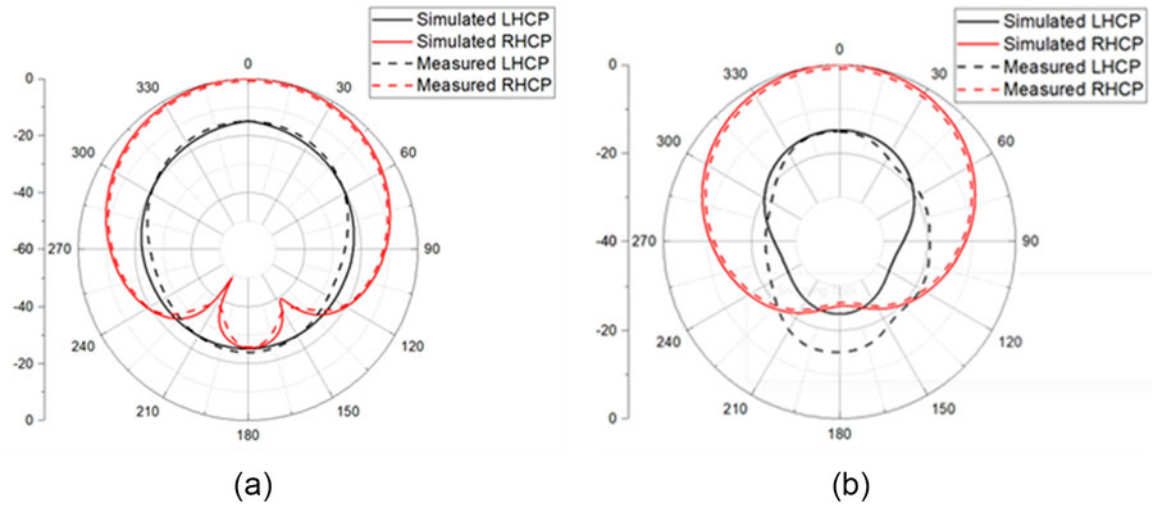


Figure 6. Measured and simulated radiation patterns at 2.4 GHz: (a) $\varphi = 0°$ and (b) $\varphi = 90°$.

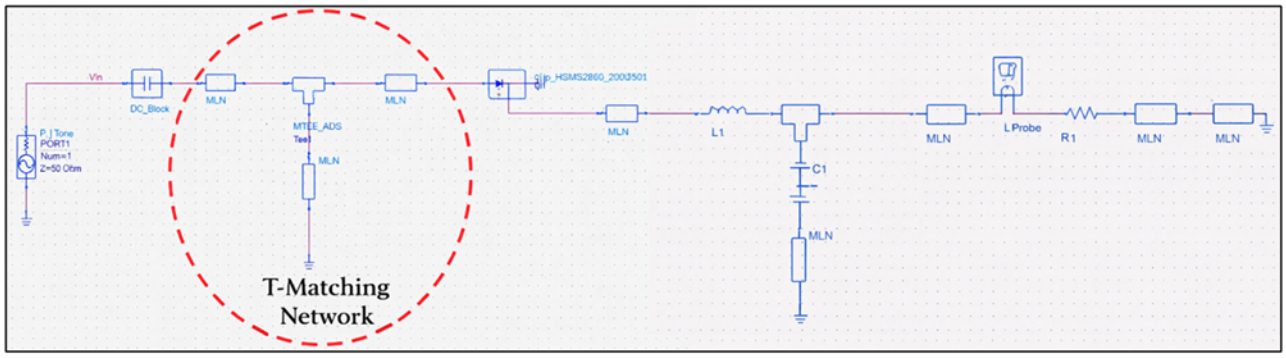


Figure 7. Schematic of the proposed rectifier.

implemented on an FR-4 substrate featuring a relative permittivity (ε_r) of 4.4, loss tangent (tan δ) of 0.02, and a thickness (h) of 1.6 mm.

Figure 8(a) demonstrates the dimensions and blueprint specifications of reported rectifier. The proposed rectifier converts RF energy from the connected antenna into usable electrical power. This method employs the rectification concept, in which alternating current signals from the RF source are changed to DC output. In the rectenna design, the capacitor (C) serves two purposes. First, it provides a smooth DC output voltage by avoiding the higher-order modes formed by the nonlinear diode. Furthermore, the shunt connection between the load impedance and the capacitor acts as a low-pass filter, created by the 1 kΩ load resistance.

Figure 8(b) illustrates the prototype of the fabricated rectifier. It also includes a T-matching network designed to transfer the maximum amount of power from the CP antenna to the load resistance. For the optimal load impedance of 1 kΩ, the DC voltage versus input power has been analyzed for a load sweep ranging from 500 Ω to 2000 Ω. In addition, for a wider load sweep from 500 Ω to 4000 Ω, the PCE has been evaluated as a function of input power. The corresponding results are presented in Figures 11(b) and (c). Additionally, the capacitor placed near the load resistance functions as a storage capacitor.

Measurement results

The RF-DC efficiency can be expressed as a ratio of output DC power to input RF power. The increase in DC power enhances the voltage drop through the load resistance at low RF input power, thus increasing the efficiency, which is directly proportionate to the output DC power. The efficiency (η) of the rectifier is calculated as

$$\eta = \frac{P_{DC}}{P_{in}}, \tag{5}$$

$$P_{DC} = \frac{V_{DC}^2}{R_L}, \tag{6}$$

where P_{in} is the RF input power, V_{DC} is the voltage across load resistance, P_{DC} is the output DC voltage and R_L is the load resistor.

Figure 9 illustrates the real and imaginary impedance plots with FSS structure. The graph displays the frequency-dependent impedance behavior, indicating that the antenna does not maintain 50 Ω across the band. The real impedance ranges from 30 Ω to 55 Ω, while the imaginary impedance ranges from −40 Ω to +10 Ω, demonstrating reactive behavior and validating impedance matching across the operating band.

To achieve optimal performance, the impedance of the RF rectifier should match that of the antenna, typically set to 50 Ω.

https://doi.org/10.1017/S1759078726103158 Published online by Cambridge University Press

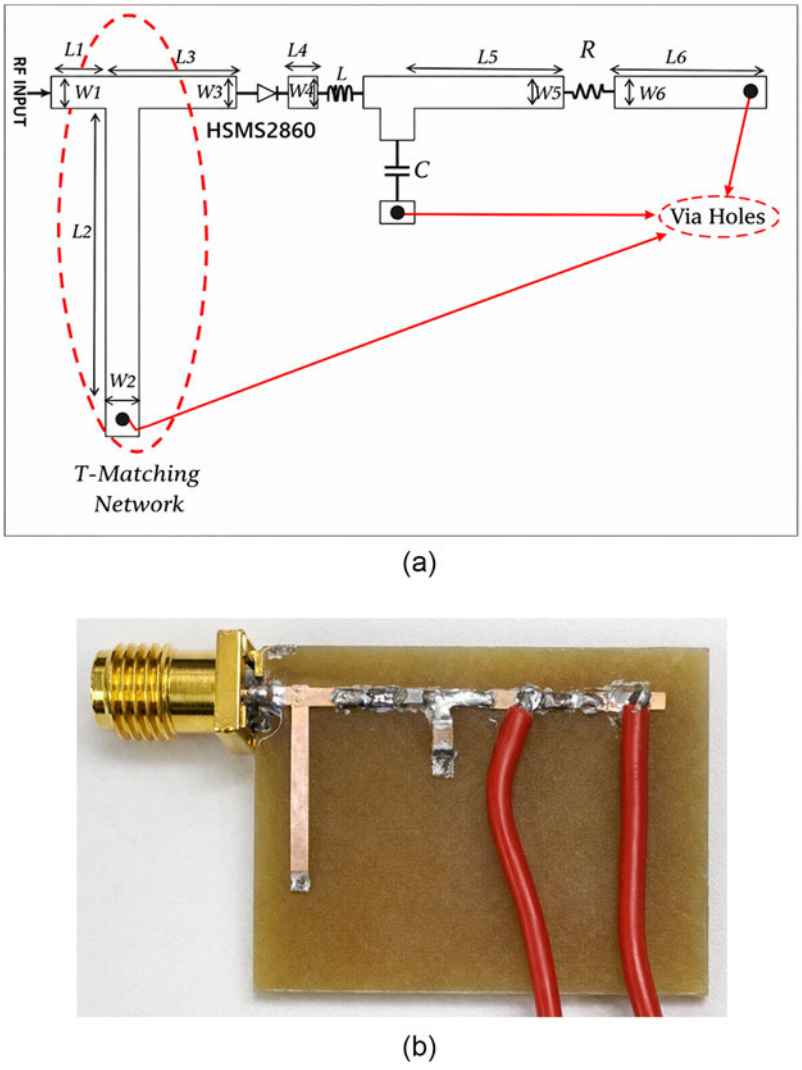


Figure 8. Proposed rectifier: (a) dimensions and design specifications ($W = 25$ mm, $L = 19$ mm, $L1 = 2$ mm, $W1 = 3$ mm, $L2 = 10$ mm, $W2 = 3$ mm, $L3 = 5$ mm, $W3 = 3$ mm, $L4 = 2$ mm, $W4 = 2$ mm, $L5 = 7$ mm, $W5 = 3$ mm, $L6 = 3$ mm, $W6 = 3$ mm) and (b) photograph of the rectifier prototype.

Impedance matching confirms optimal power transfer from the antenna to the rectifier, while also reducing signal reflections and increasing energy harvesting efficiency. To accurately capture the nonlinear behavior of the rectifier impedance under varying input power levels using a frequency sweep, Figure 10 shows the variation of rectifier impedance with frequency and input power. Figure 10(a) shows that the rectifier impedance is frequency dependent, with 225 Ω at 2.1 GHz, ∼50 Ω at 2.4 GHz and gradually decreasing to below 50 Ω above 2.6 GHz as diode conduction increases. This behavior confirms the nonlinear nature of the rectifier and the importance of frequency-optimized matching.

Figure 10(b) shows the variation of input impedance of the rectifier with input power level, emphasizing the nonlinear behavior typical of diode-based rectifier circuits. When the input power ranges from −30 dBm to −20 dBm, the impedance is high, ranging from 150 Ω to 180 Ω due to the diode not fully turned on condition. The rectifier has an impedance of ∼50 Ω when the input power is −10 dBm. As input power increases, diode conduction reduces impedance to 35–45 Ω at 0 to +5 dBm. This power-dependent impedance variation confirms that rectifier matching must be designed considering nonlinear operation instead of a single fixed impedance value.

Figure 11(a) shows the measurement and simulated return loss parameters of the suggested rectifier. Inconsistencies in the

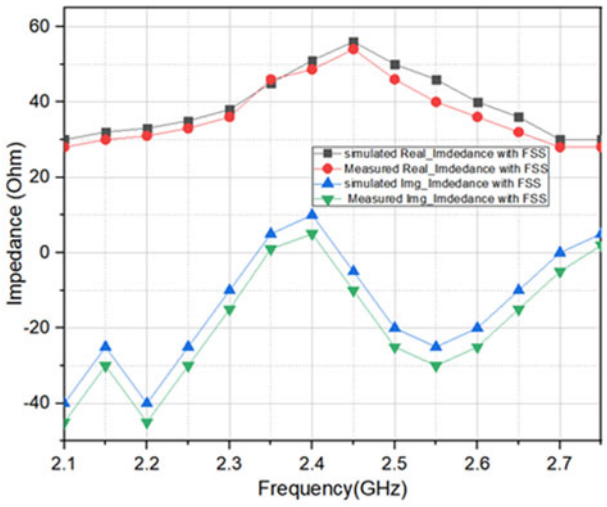


Figure 9. Real and imaginary impedance of the proposed antenna.

https://doi.org/10.1017/S1759078726103158 Published online by Cambridge University Press

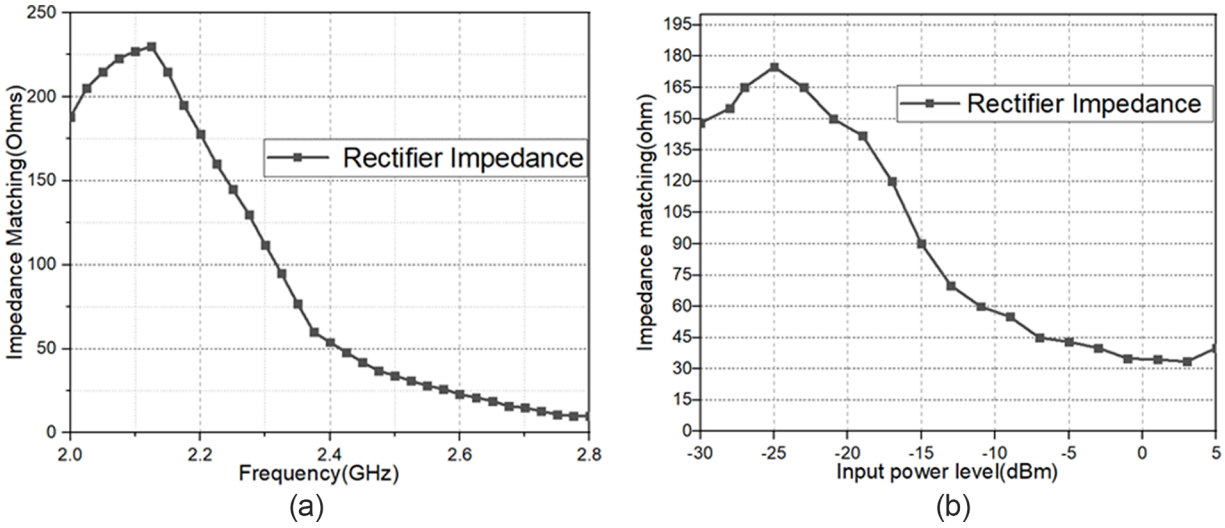


Figure 10. Rectifier circuit impedance matching: (a) variation of impedance and frequency and (b) variation of impedance and input power level at 2.4 GHz.

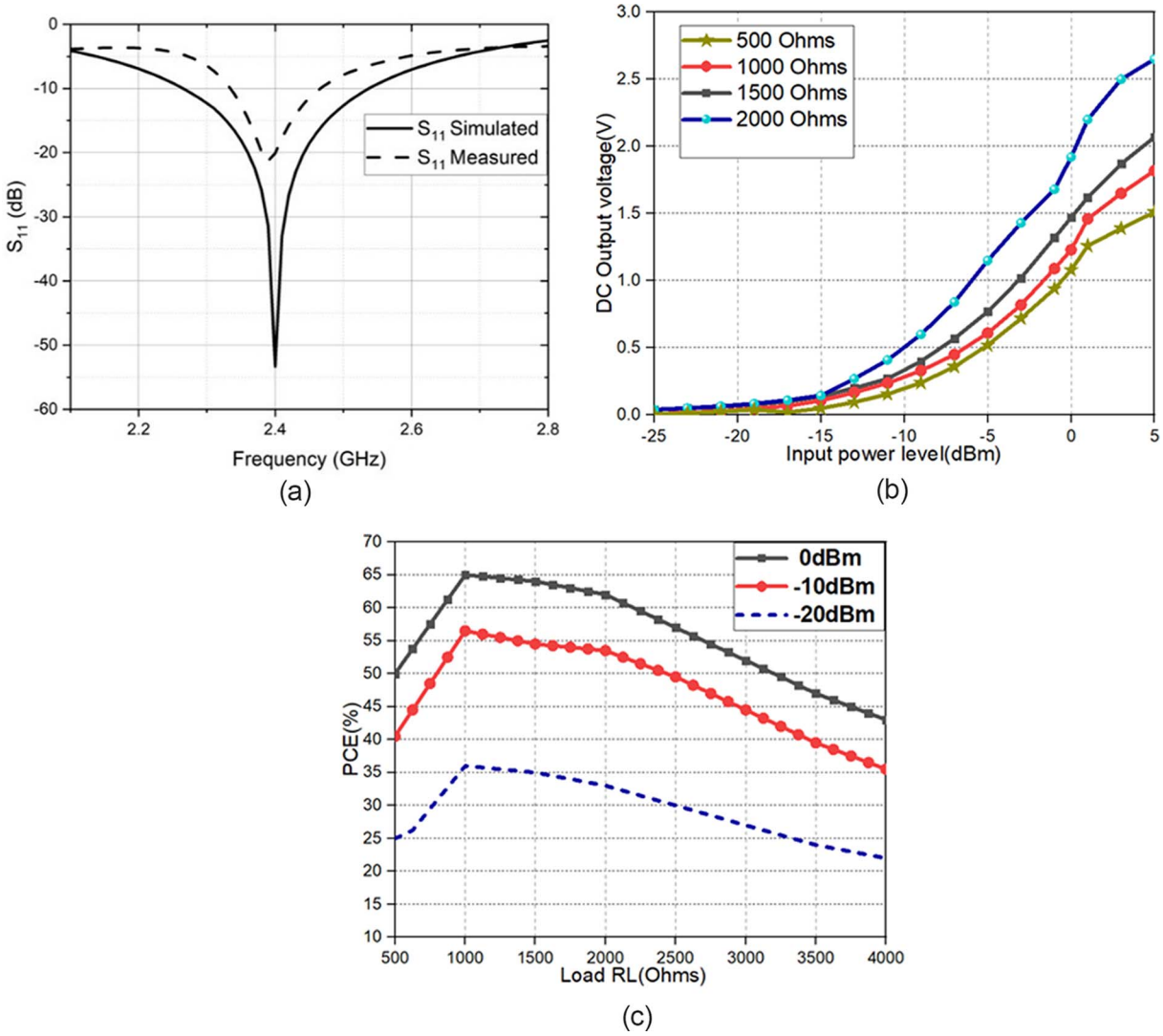


Figure 11. (a) Simulated and measured S-parameters, (b) simulated DC output voltage versus input power levels for various load resistances, and (c) simulated PCE versus load resistance at various input power levels.

https://doi.org/10.1017/S1759078726103158 Published online by Cambridge University Press

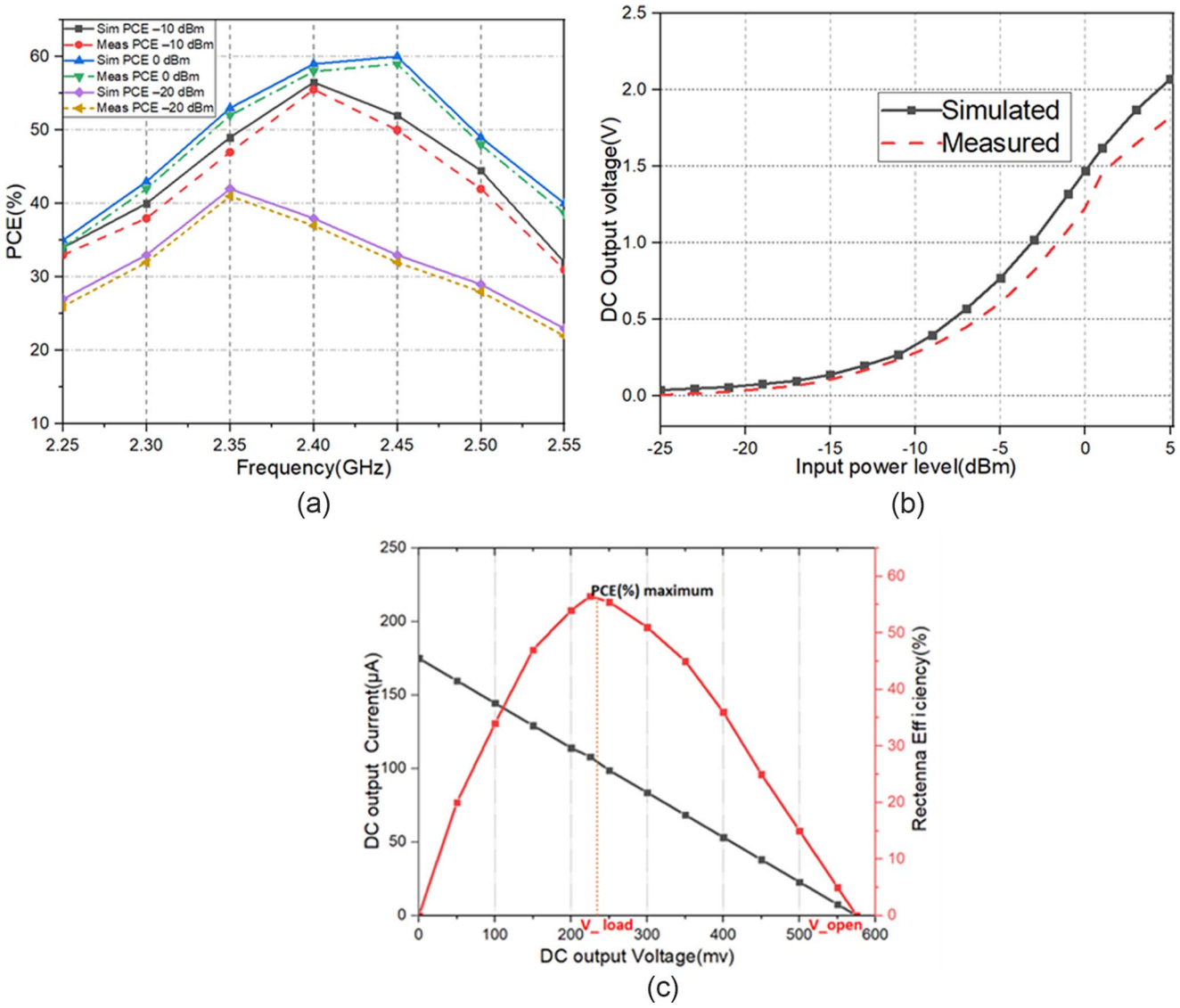


Figure 12. (a) RF-to-DC conversion efficiency at an input power sweep, (b) DC output voltage versus input power at 1000 Ω load resistor, and (c) variation of DC output current, PCE, and DC output voltage.

measurement data are attributed to environmental losses such as absorption, scattering, and reflection. The propagation of electromagnetic waves is influenced by a variety of factors, including material properties, interference, and spatial configuration, all of which can cause performance losses in rectifiers. Shielding techniques, improved antenna design, and rectifier circuitry refinement can all help to reduce environmental losses while increasing system performance.

Figure 11(b) shows that the DC output voltage increases nonlinearly with input power. Higher load resistances (1500–2000 Ω) result in significantly higher output voltage due to improved power-to-voltage conversion. The 1000 Ω load consistently produces a higher DC output voltage than 500 Ω and slightly lower than 1500–2000 Ω, indicating near-optimal voltage conversion with minimal voltage drop or mismatch.

The PCE versus load resistance graph shows that all three input power levels (0 dBm, −10 dBm, and −20 dBm) achieve their maximum efficiency at 1000 Ω, indicating that this load achieves the most effective power extraction from the rectifier in Figure 11(c). The optimum load is 1000 Ω, which provides optimal impedance matching, minimizes conduction losses, and maintains the voltage–current operating point of the rectifier across different input power levels.

Figure 12(a) depicts simulated and measured RF-to-DC conversion efficiencies at various input power levels. At 2.4 GHz and an input power of −10 dBm, the rectifier achieves a measured PCE of around 56.5%, while the simulated value is slightly higher at 62.5%. When the input power is reduced to −20 dBm, the conversion efficiency drops significantly, reaching only around 40%, highlighting the rectifier's reduced performance at lower power levels.

Figure 12(b) shows the simulated and measured DC output voltages versus the available input power at 2.4 GHz. At −10 dBm input power, the rectifier generates approximately 0.238 V. As the input power increases from −10 dBm to 0 dBm, the output voltage increases significantly, reaching nearly 1.5 V, demonstrating a

https://doi.org/10.1017/S1759078726103158 Published online by Cambridge University Press

Table 1. Comparison of the suggested RF rectifier to related works

Ref.	Antenna size ($\lambda_0 \times \lambda_0$)	Resonant frequency (GHz)	Efficiency (η)	Topology	Polarization	Gain (dBi)	HPBW (°)	PCE (%)	Input power for PCE (dBm)
[25]	$0.92\lambda_0 \times 0.744\lambda_0$	2.4	52	Modified bridge rectifier	LP	4.7	–	52	~10 (0.15 mW/cm^2)
[26]	$0.76\lambda_0 \times 0.76\lambda_0$	2.4	56	–	CP	4.7	–	69 (peak efficiency)	~20 (power density context)
[27]	$0.4\lambda_0 \times 0.092\lambda_0$	2.4	40	Matching network	LP	0	–	58	0
[28]	$0.84\lambda_0 \times 0.84\lambda_0$	2.2	50	Voltage doubler	CP	7	–	40	–
[29]	$5.6\lambda_0 \times 2.22\lambda_0$	31.5	12	Voltage doubler	LP	8	–	12	9.5
Prop.	$0.4\lambda_0 \times 0.32\lambda_0$	2.4	56.5	Series	CP	6.5	73	56.5	−10

Note: LP = linearly polarized; CP = circularly polarized.

nonlinear improvement in rectification efficiency at higher power levels.

Figure 12(c) shows the DC output performance of the rectifier under varying load conditions, focusing on the internal behavior of the rectenna system. The DC I–V curve (black) shows a nearly linear decline in output current as the output voltage increases, which is consistent with the behavior of a diode rectifier under RF excitation. When the load resistance is low, the rectifier produces high current but low voltage. As the load resistance increases, the operating point shifts toward higher voltage at the expense of current, eventually reaching the open-circuit voltage (≈575 mV) where the current is zero. However, the PCE curve (red) has a distinct maximum that corresponds to the maximum power point. The peak occurs at $V_{DC} \approx 238$ mV, when the DC output power reaches its maximum voltage and current. The location of this peak indicates that the optimum load voltage is close to half of the open-circuit voltage, which is consistent with the theoretical condition for maximum power transfer in nonlinear rectifying circuits, where the effective load resistance matches the rectifier's internal dynamic resistance.

This relationship confirms proper impedance interaction between the rectifier, matching network, and load and emphasizes the importance of selecting a load value that positions the operating point near the maximum power point to maximize harvesting efficiency.

Table 1 compares the properties of the suggested rectifier to rectenna designs published in the literature. The comparison shows that the proposed rectifier outperforms the reported rectifier designs, making it more advantageous and useful for RF energy harvesting.

Pentagonal antenna array

Figure 13 depicts the proposed 3D pentagonal antenna array structure, along with FSS. The array consists of five antenna elements and an FSS, each with a 72° coverage angle. The 3D pentagonal antenna array allows for 360° collection of ambient signals, while the CP antenna ensures RF signal sensing in the full azimuth plane, making it suitable for real-world implementation.

Figure 14(a) depicts the reflection coefficients of the four array elements at 2.4 GHz, demonstrating good impedance matching at all ports. Figure 14(b) shows an axial ratioof less than 3 dB at 2.4 GHz frequency, indicating that the pentagonal antenna array has good circular polarization. The pentagonal radiating element at 2.4 GHz has a peak gain of 6.5 dBi, indicating that there is no hidden spot in the antenna's coverage and signal is effectively received from all directions, enhancing its suitability for energy harvesting applications.

Conclusion

The paper presents a CP rectenna operating at 2.4 GHz. A pentagonal-shaped antenna with a simple geometry is proposed, loaded with circular slots to achieve circular polarization. Also, an FSS layer is designed with hexagonal-shaped unit cells to enhance working in terms of gain of the pentagonal-shaped antenna. A T-matching system is used with reported rectifier to improve changeover efficiency over a wide input power range. At 0 dBm input power, the rectenna offers a DC output voltage of 1.5 V, while at −10 dBm input power, the voltage is 0.238 V. The maximum RF-to-DC translation efficiency is 56.5% at −10 dBm input power. The

https://doi.org/10.1017/S1759078726103158 Published online by Cambridge University Press

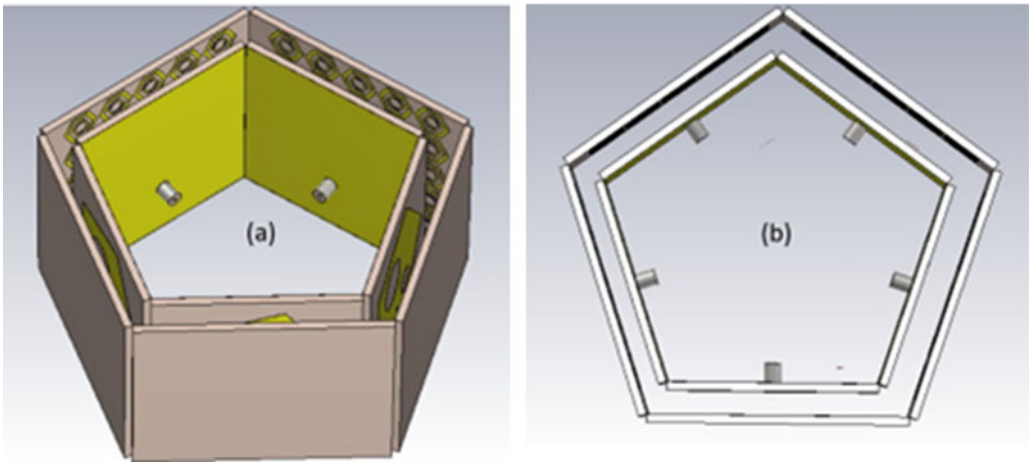


Figure 13. Proposed 3D pentagonal antenna array: (a) side view and (b) top view.

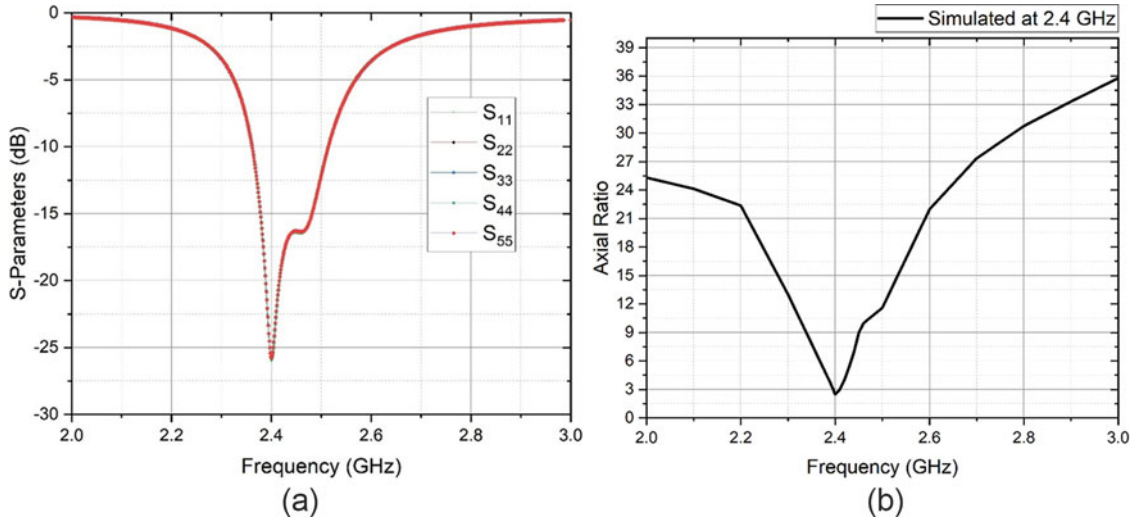


Figure 14. 3D pentagonal antenna array: (a) S-parameters and (b) axial ratio.

results show that the simulated and measured data agree very well. In addition, a unique CP pentagonal antenna array with five antennas and five FSS layers is proposed for 360° ambient RF energy harvesting applications.

Competing interests. The author(s) declare none.

References

1. **Niotaki K, Carvalho NB, Georgiadis A, Gu X, Hemour S, Wu K, Matos D, Belo D, Pereira R, Figueiredo R, Chaves H, Mendes B, Correia R, Oliveira ASR, Palazzi V, Alimenti F, Mezzanotte P, Roselli L, Benassi F, Costanzo A, Masotti D, Paolini G, Eid A, Hester J, Tentzeris MM and Shinohara N** (2023) RF energy harvesting and wireless power transfer for energy autonomous wireless devices and RFIDs. *IEEE Journal of Microwaves* **3**, 763–782. https://doi.org/10.1109/JMW.2023.3255581
2. **Singh N, Kanaujia BK, Beg MT, Mainuddin and Kumar S** (2019) A triple band circularly polarized rectenna for RF energy harvesting. *Electromagnetics* **39**(7), 481–490. https://doi.org/10.1080/02726343.2019.1658164
3. **Singh N, Kanaujia BK, Beg MT, Mainuddin, Kumar S, Choi HC and Kim KW** (2019) Low profile multiband rectenna for efficient energy harvesting at microwave frequencies. *International Journal of Electronics* **106**(12), 2057–2071. https://doi.org/10.1080/00207217.2019.1636302
4. **Singh N, Khan T, Kumar S, Kanaujia BK, Choi HC, Kim KW, Rambabu K, Rengarajan SR and Kishk AA** (2024) Ultra-thin flexible rectenna integrated with power management unit for wireless power harvester/charging of smartwatch/wristband. *Scientific Reports* **14**, 7447. https://doi.org/10.1038/s41598-024-57639-1
5. **Xu Z, Khalifa A, Mittal A, Nasrollahpourmotlaghzanjani M, Etienne-Cummings R, Xiang Sun N, Cash SS and Shrivastava A** (2022) Analysis and design methodology of RF energy harvesting rectifier circuit for ultra-low power applications. *IEEE Open Journal of Circuits and Systems* **3**, 82–96. https://doi.org/10.1109/OJCAS.2022.3169437
6. **Sun H, Huang J and Wang Y** (2022) An omnidirectional rectenna array with an enhanced RF power distributing strategy for RF energy harvesting. *IEEE Transactions on Antennas and Propagation* **70**, 4931–4936. https://doi.org/10.1109/TAP.2021.3138542
7. **Munir B and Dyo V** (2018) On the impact of mobility on battery-less RF energy harvesting system performance. *Sensors* **18**, 3597. https://doi.org/10.3390/s18113597
8. **Derbal MC and Nedil M** (2020) A high gain dual band rectenna for RF energy harvesting applications. *Progress in Electromagnetics Research Letters* **90**, 29–36. https://doi.org/10.2528/PIERL19122604
9. **Wang T, Huang K, Liu W, Hou J and Zhang Z** (2022) A hybrid solar-RF energy harvesting system based on tree-shaped antenna array.

https://doi.org/10.1017/S1759078726103158 Published online by Cambridge University Press

International Journal of RF and Microwave Computer-Aided Engineering **32**, e23301. 10.1002/mmce.23301.

10. **Shen S, Chiu CY and Murch RD** (2017) A dual-port triple-band l-probe microstrip patch rectenna for ambient RF energy harvesting. *IEEE Antennas and Wireless Propagation Letters* **16**, 3071–3074. https://doi.org/10.1109/LAWP.2017.2761397
11. **Ojha SS, Mishra S, Dhakad B and Singh BP** (2024) Dual-wideband rectenna for RF energy harvesting from 5G and WIMAX. *International Journal of Electronics* **112**(7), 1476–1493. https://doi.org/10.1080/00207217.2024.2390153
12. **Li J, Wu S, Li Z, Cao Y and Yan S** (2024) Robust broadband dual-polarized rectenna with high conversion efficiency. *AEU - International Journal of Electronics and Communications* **179**, 155294. https://doi.org/10.1016/j.aeue.2024.155294
13. **Kumar M, Kumar S and Sharma A** (2022) Dual-purpose planar radial-array of rectenna sensors for orientation estimation and RF-energy harvesting at IoT nodes. *IEEE Microwave and Wireless Components Letters* **32**, 245–248. https://doi.org/10.1109/LMWC.2022.3145196
14. **Srivastava VK, Kumar S and Sharma A** (2021) 3D polarized field-forming for mitigation of angular misalignment problem in microwave power transfer systems. In *Proceedings of the 2021 IEEE 19th International Symposium on Antenna Technology and Applied Electromagnetics (ANTEM)*. Winnipeg, MB, Canada: IEEE, pp. 1–2.
15. **Halimi MA, Shome PP, Khan T and Rengarajan SR** (2023) Efficient single and broadband microwave rectifiers for RFEH/WPT enabled low power 5G sub-6 GHz devices. *AEU-International Journal of Electronics and Communications* **165**, 154645.
16. **Sang J, Qian L, Wang X and Shi G** (2025) A dual-band omnidirectional rectenna for radio-frequency energy harvesting applications. *Microelectronics Journal* **156**, 106533. https://doi.org/10.1016/j.mejo.2024.106533
17. **Zhu L, Zhang J, Han W, Xu L and Bai X** (2019) A novel RF energy harvesting cube based on air dielectric antenna arrays. *International Journal of RF and Microwave Computer-Aided Engineering* **29**, e21636. https://doi.org/10.1002/mmce.21636
18. **Sedeek A, Tammam E and Hasaneen ES** High efficiency 2.45 GHz low power hybrid junction rectifier for RF energy harvesting (2018) Alexandria, Egypt: IEEE, pp. 147–150.
19. **Elzwawi GH, Kesavan A, Alwahishi R and Denidni TA** (2020) A new corner-reflector antenna with tunable gain based on active frequency selective surfaces. *IEEE Open Journal of Antennas and Propagation* **1**, 88–94. https://doi.org/10.1109/OJAP.2020.2979053
20. **Liu N, Liu X, Sheng X, Li X and Ding H** (2024) A dual-polarized, notched electromagnetic energy harvester array based on FSS. *IEEE Antennas and Wireless Propagation Letters* **23**(11), 3782–3786. https://doi.org/10.1109/LAWP.2024.3379221
21. **Ferreira D, Sismeiro L, Ferreira A, Caldeirinha RF, Fernandes TR and Cuiñas I** (2016) Hybrid FSS and rectenna design for wireless power harvesting. *IEEE Transactions on Antennas and Propagation* **64**, 2038–2042. https://doi.org/10.1109/TAP.2016.2536168
22. **Khajevandi S, Oraizi H, Amini A and Poordaraee M** (2019) Design of miniaturised-element FSS based on 2.5-dimensional closed-loop Hilbert fractal. *IET Microwaves, Antennas & Propagation* **13**, 742–747. https://doi.org/10.1049/iet-map.2018.5036
23. **Sung Y** (2018) Axial ratio-tuned circularly polarized square patch antenna with long stubs. *International Journal of Antennas and Propagation* **2018**, 7068560 doi:10.1155/2018/7068560
24. **Shakhirul M, Jusoh M, Ismail A, Kamarudin M, Yahya R, Yasin M and Sabapathy T** (2014) 1.575 GHz circular polarization wearable antenna with three different substrate materials. In *Proceedings of the 2014 IEEE Asia-Pacific Conference on Applied Electromagnetics (APACE)*. Johor Bahru, Malaysia: IEEE, pp. 43–46.
25. **Wagih M, Hilton GS, Weddell AS and Beeby S** (2020) Broadband millimeter-wave textile-based flexible rectenna for wearable energy harvesting. *IEEE Transactions on Microwave Theory & Techniques* **68**, 4960–4972. https://doi.org/10.1109/TMTT.2020.3018735
26. **Mahfoudi H, Tellache M and Takhedmit H** (2019) A wideband rectifier array on dual-polarized differential-feed fractal slotted ground antenna for RF energy harvesting. *International Journal of RF and Microwave Computer-Aided Engineering* **29**, 1–9. https://doi.org/10.1002/mmce.21775
27. **Eid A, Hester JG, Costantine J, Tawk Y, Ramadan AH and Tentzeris MM** (2020) A compact source-load agnostic flexible rectenna topology for IoT devices. *IEEE Transactions on Antennas and Propagation* **68**, 2621–2629. https://doi.org/10.1109/TAP.2019.2955211
28. **Takhedmit H, Cirio L, Bellal S, Delcroix D and Picon O** (2012) Compact and efficient 2.45 GHz circularly polarised shorted ring-slot rectenna. *Electronics Letters* **48**, 253–254.
29. **Takhedmit H, Merabet B, Cirio L, Allard B, Costa F, Vollaire C and Picon O** (2010) A 2.45-GHz low cost and efficient rectenna. In *Proceedings of the Fourth European Conference on Antennas and Propagation*. Barcelona, Spain: IEEE, pp. 1–5.

https://doi.org/10.1017/S1759078726103158 Published online by Cambridge University Press